Observations of core toroidal rotation reversals in Alcator C-Mod ohmic L-mode plasmas

To cite this article: J.E. Rice et al 2011 Nucl. Fusion **51** 083005

View the article online for updates and enhancements.

Observations of core toroidal rotation reversals in Alcator C-Mod ohmic L-mode plasmas

J.E. Rice, B.P. Duval[1], M.L. Reinke, Y.A. Podpaly, A. Bortolon[1,a], R.M. Churchill, I. Cziegler, P.H. Diamond[2], A. Dominguez, P.C. Ennever, C.L. Fiore, R.S. Granetz, M.J. Greenwald, A.E. Hubbard, J.W. Hughes, J.H. Irby, Y. Ma, E.S. Marmar, R.M. McDermott[b], M. Porkolab, N. Tsujii and S.M. Wolfe

Plasma Science and Fusion Center, MIT, Cambridge, MA, USA
[1] Ecole Polytechnique Federale de Lausanne, Centre de Recherches en Physique des Plasmas, Lausanne, Switzerland
[2] University of California, San Diego, La Jolla, CA, USA

Abstract

Direction reversals of intrinsic toroidal rotation have been observed in Alcator C-Mod ohmic L-mode plasmas following modest electron density or toroidal magnetic field ramps. The reversal process occurs in the plasma interior, inside of the $q = 3/2$ surface. For low density plasmas, the rotation is in the co-current direction, and can reverse to the counter-current direction following an increase in the electron density above a certain threshold. Reversals from the co- to counter-current direction are correlated with a sharp decrease in density fluctuations with $k_R \geqslant 2\,\mathrm{cm}^{-1}$ and with frequencies above 70 kHz. The density at which the rotation reverses increases linearly with plasma current, and decreases with increasing magnetic field. There is a strong correlation between the reversal density and the density at which the global ohmic L-mode energy confinement changes from the linear to the saturated regime.

(Some figures in this article are in colour only in the electronic version)

1. Introduction

Until recently, plasma rotation and momentum transport in tokamaks have not received as much attention as particle and energy transport [1]. Since velocity shear is important for its role in reducing turbulence [2, 3] and plasma rotation can suppress deleterious magnetohydrodynamic modes [4], it is important to address these topics. Usually rotation is generated externally by neutral beam injection, but since momentum input from beams is expected to be low in ITER and future devices, other methods are under consideration. This includes taking advantage of intrinsic rotation, the self-generated flow which arises in the absence of external momentum input. Intrinsic rotation in H-mode and other enhanced confinement regimes is generally directed co-current and has been found to have a relatively simple global scaling [5], with the Mach number proportional to the plasma pressure. For plasmas with significant ripple, this scaling may not hold [6]. In contrast, the intrinsic rotation in L-mode plasmas has a complicated dependence on plasma parameters [6–10]. In fact, rotation inversions or reversals have been observed in TCV and C-Mod [8, 9, 11–13], where the core intrinsic velocity abruptly switches direction, with negligible effect on other macroscopic plasma parameters. Rotation reversals have been induced with changes in density, plasma current, magnetic field and plasma shape. Since the rotation in L-mode plasmas is related to the H-mode power threshold ([8] and references therein), it is important to understand L-mode rotation in its own right. The purpose of this study is to shed light on this curious reversal phenomenon. In section 2 the experimental setup on Alcator C-Mod will be described, followed by presentation of reversal time histories with density and magnetic field ramps and scalings with plasma current and magnetic field in section 3. Velocity profile evolution is the focus of section 4. Observations of turbulence changes during reversals will be shown in section 5, with discussion and conclusions presented in section 6.

2. Experimental setup

These experiments were performed on the Alcator C-Mod tokamak [14], a compact ($R = 0.67\,\mathrm{m}$, $a \sim 0.21\,\mathrm{m}$), high

---

magnetic field ($B_T \leqslant 8$ T) device with molybdenum plasma facing components. For the plasma conditions considered here, the electron density was between 0.2 and 2.0×10^{20} m^{-3}, the plasma current ranged from 0.4 to 1.4 MA and the toroidal magnetic field was between 2.7 and 7.0 T ($2.6 \leqslant q_{95} \leqslant 7.2$). Discharges were operated in the lower single null (LSN), upper single null (USN) and inner wall limited magnetic field configurations, without auxilliary heating. Plasma elongation ranged from 1.53 to 1.69, upper triangularity was between 0.22 and 0.33 for LSN and from 0.60 to 0.75 for USN, and lower triangularity ranges were 0.36–0.50 for LSN and 0.28–0.32 for USN. All discharges reported here were in the ohmic L-mode confinement regime.

Central rotation velocities were measured using a tangentially viewing von Hamos type x-ray spectrometer [15], and complete core rotation profiles were obtained utilizing an imaging x-ray spectrometer system [16]. Typical integration time for both spectrometer systems is 20 ms, and both have ~1 cm spatial resolution. For the imaging system, there is no external absolute wavelength calibration; calibration was achieved from a comparison with the von Hamos spectrometer which is absolutely calibrated and by operating with locked modes which brake the core rotation [17]. If the rotation profile is not stagnant across the entire profile ($V_{Tor}(r) = 0$) during a locked mode, then the details of the shapes of the velocity profiles in the outer regions presented in section 4 may be different. Changes in the velocity profiles during the reversal process are accurate to better than 10%. All central velocities presented here were from the imaging system. Edge rotation velocity profiles were obtained with a charge exchange recombination spectroscopy (CXRS) system [18, 19] using a perpendicular diagnostic neutral beam (DNB). Typical integration time for the CXRS system is 5 ms, and spatial resolution is 1.5 mm. There is very good agreement in the velocity profiles from the x-ray and CXRS systems in the outer regions of the plasma where the coverage overlaps. Electron density and temperature profiles were measured from Thomson scattering [18]. Density fluctuations were observed with phase contrast imaging (PCI), gas puff imaging and reflectometer systems [18].

3. Rotation reversal time histories and scalings

The complicated dependence of core intrinsic toroidal rotation on electron density in ohmic L-mode plasmas has been previously demonstrated for specific discharge conditions [8, 9]: 5.4 T, 0.8 MA, LSN and USN. This parameter set has been expanded to other plasma currents and magnetic fields in the current study. Shown for comparison in figure 1 is the scaling of the central toroidal rotation velocity as a function of electron density for a series of individual 5.2 T, LSN ohmic discharges at plasma currents of 0.6 and 1.0 MA. Throughout this paper positive velocity denotes co-current and negative velocity denotes counter-current. For the 0.6 MA cases, there is very little dependence on electron density above 0.6×10^{20} m^{-3}, and the rotation is in the counter-current direction, with values around -20 km s^{-1}. As the density is lowered below 0.6×10^{20} m^{-3}, the rotation abruptly changes to the co-current direction. Similar behaviour is observed at plasma currents of 1.0 MA, but the density at which the
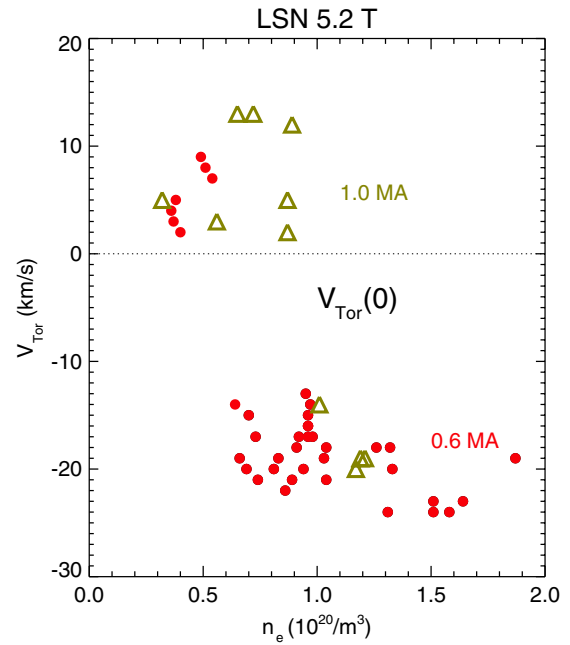

Figure 1. The central rotation velocity as a function of average electron density for LSN, 5.2 T ohmic discharges with plasma currents of 0.6 MA (dots) and 1.0 MA (triangles). Positive velocity denotes co-current while negative velocity denotes counter-current.
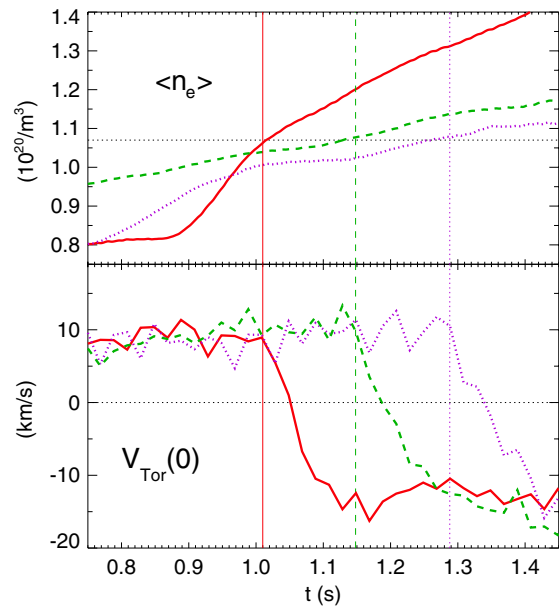

Figure 2. Time histories of the average electron density (top) and central toroidal rotation velocity (bottom) for LSN 1.05 MA 5.4 T ($q_{95} = 3.2$) discharges with different density ramps. The dotted horizontal line in the top frame represents an average density of 1.07×10^{20} m^{-3}. Vertical lines indicate the initiation times of the three reversals.

rotation reversal occurs is higher, around 1×10^{20} m^{-3}. This reversal of the toroidal rotation direction can be observed dynamically during the course of a single discharge by utilizing density ramps [9, 11]. Shown in figure 2 are the time histories of three LSN, 5.4 T, 1.05 MA ohmic L-mode discharges ($q_{95} \sim 3.2$) with different upward density ramps. In all
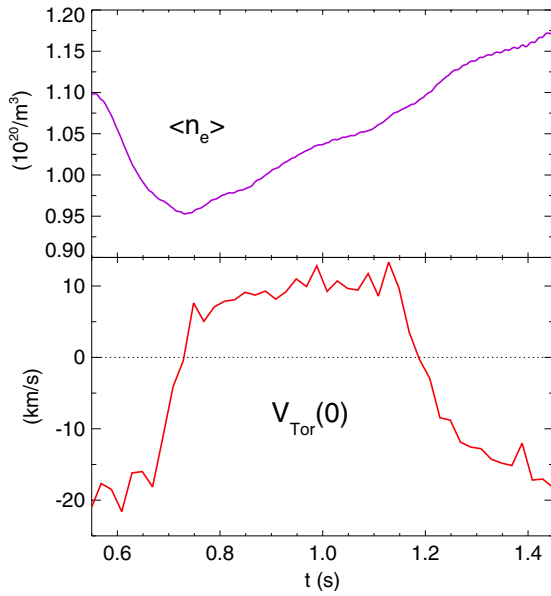
Figure 3. Time histories of the average electron density (top) and central toroidal rotation velocity (bottom) for a LSN 1.05 MA 5.4 T ($q_{95} = 3.2$) discharge with two reversals.

Figure 4. The discharge trajectory in the n_e–V_{Tor} plane for the plasma of figure 3. Points are separated by 20 ms.

Figure 5. Time histories of q_{95} (top frame), average electron density (middle frame) and central toroidal rotation velocity (bottom frame) for 5.4 T LSN discharges with plasma currents of 0.64 MA (dotted), 0.80 MA (dashed) and 1.06 MA (solid).

three cases, the central toroidal rotation velocity began to drop from ∼+10 km s^{-1} (co-current) as the electron density passed through ∼1.07 × 10^{20} m^{-3}, eventually settling to ∼−15 km s^{-1} (counter-current). This rotation reversal usually occurs on a time scale comparable to the L-mode momentum confinement time (∼25 ms) [17, 20], although some reversals develop more slowly. The initiation of rotation reversals is quite sensitive to the value of the electron density, as is demonstrated in figure 3. This plasma experienced two reversals, first from counter- to co-current beginning at 0.666 s, with a slight decrease in the electron density, and from co- to counter-current beginning at 1.146 s, with a slight density increase. Note that the scale for the density trace is greatly expanded. The overall cycle occurred with a 10% change in the electron density. The hysteresis of the process is exhibited in figure 4, which shows the discharge trajectory in the n_e–V_{Tor} plane. The magnitude of the rotation excursion was ∼30 km s^{-1}. Whether rotation reversal occurs for a given density ramp depends upon the value of the plasma current or magnetic field. Shown in figure 5 is a comparison of the time histories of three 5.4 T LSN discharges with similar density ramps, but with different plasma currents. Only the discharge at 1.06 MA underwent a rotation reversal for this particular range of densities, from 0.9 to 1.2 × 10^{20} m^{-3}. For the lower plasma currents, the density was above the 'threshold' for reversal from the co- to counter-current direction.

Rotation reversals can also be induced by ramping the plasma current or magnetic field, at fixed electron density. The latter effect is demonstrated in figure 6 where a comparison is shown of the time histories of two LSN discharges at 0.8 MA and fixed density, one of which had a ramp down and then up of the magnetic field. The discharge with the magnetic field ramp, from 4.5 to 3.0 T and back to 4.5 T, at a relatively constant density, experienced a rotation reversal during the ramp down, and a second reversal after the upward ramp. The discharge trajectory in the q_{95}–V_{Tor} plane for the plasma with
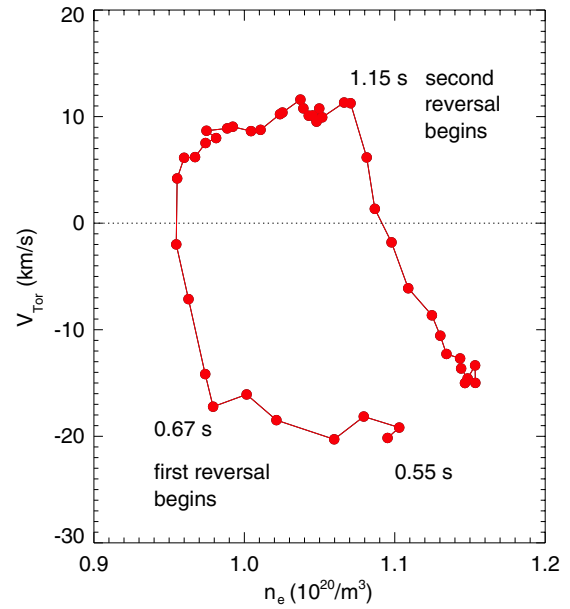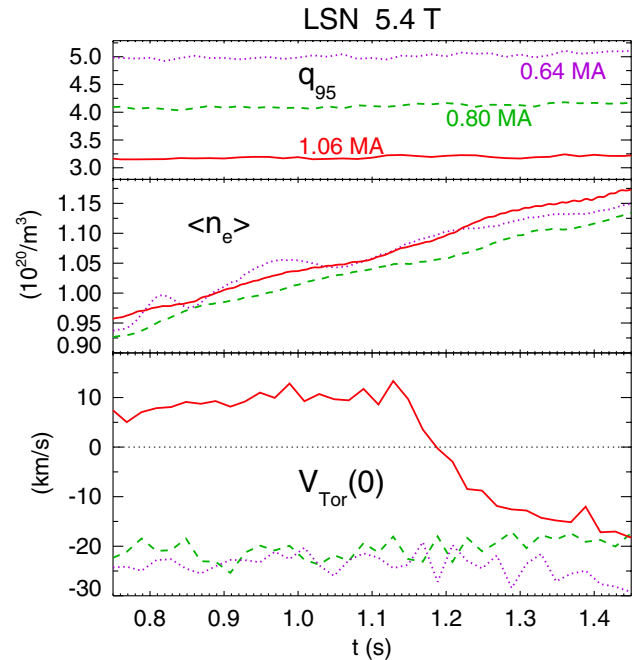
the magnetic field ramp (solid line in figure 6) is shown in figure 7. In this case there is very little hysteresis since the reversals initiated at $q_{95} \sim 3.0$ for both downward and upward magnetic field ramps. Whether this is due to slight variations in the electron density for this discharge is unknown. The overall magnitude of the velocity cycle was ∼35 km s^{-1}. The reversal density depends both on the magnetic field and plasma current independently. Shown in figure 8 is a comparison of the time histories of two 0.8 MA USN discharges, with similar
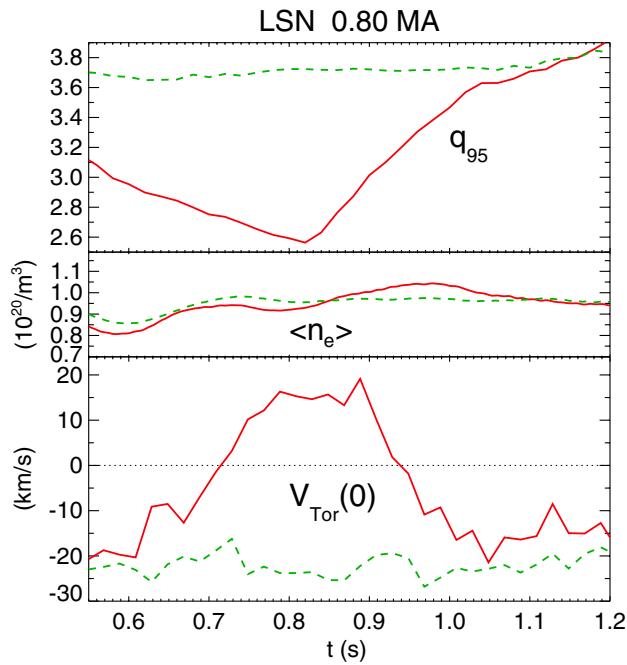
Figure 6. Time histories of 0.8 MA LSN discharges with (solid) and without (dashed) a magnetic field ramp. The same layout as in figure 5.
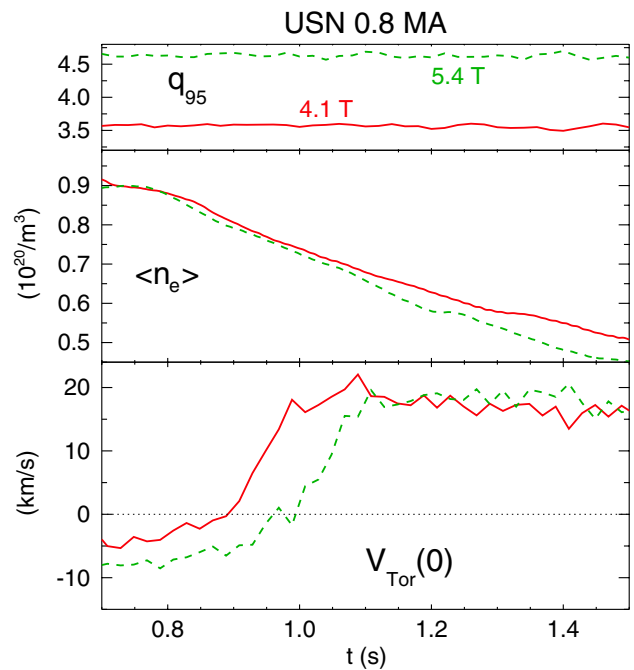

Figure 8. Time histories of 0.8 MA USN discharges at 5.4 T (dashed) and 4.1 T (solid).
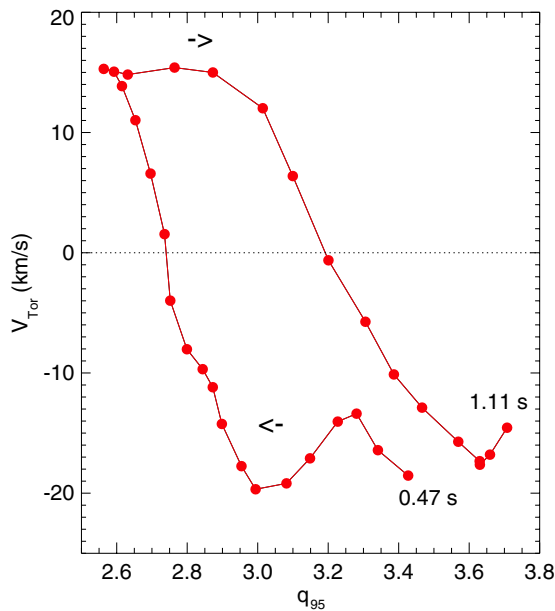

Figure 7. The discharge trajectory in the $q_{95}-V_{Tor}$ plane for the plasma shown by the solid lines in figure 6 with the magnetic field ramp. Points are separated by 20 ms. Arrows indicate temporal direction.

Figure 9. Time histories for two 4.1 T USN discharges, at 0.8 MA (solid) and 0.6 MA (dashed).

downward density ramps, at magnetic fields of 5.4 and 4.1 T. In these cases the rotation changed from counter-current to co-current as the density was ramped down. (There were earlier reversals from co- to counter- during the initial density and current ramp up as the discharges were formed.) The reversal for the higher magnetic field plasma occurred later in time, at a lower density. A related comparison is presented in figure 9, for 4.1 T USN discharges at plasma currents of 0.8 and
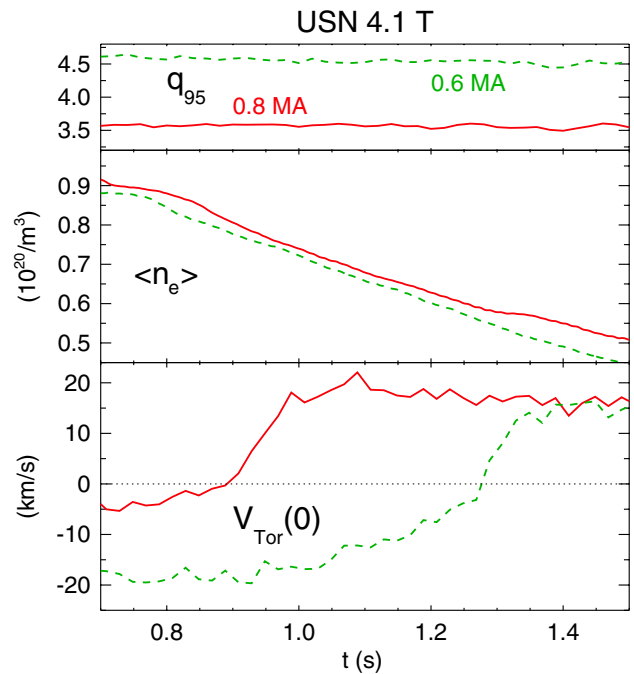
0.6 MA. For the lower current discharge, the reversal occurred later in time, at a lower density; this is consistent with the trend shown in figure 1.

A large body of rotation reversal data is summarized in figure 10 where the electron density at the time when the central rotation began to reverse is plotted as a function of plasma current, sorted for different magnetic fields. For 5.4 T discharges, there is a linear increase of the reversal density with plasma current over a factor of three. These points are a mix
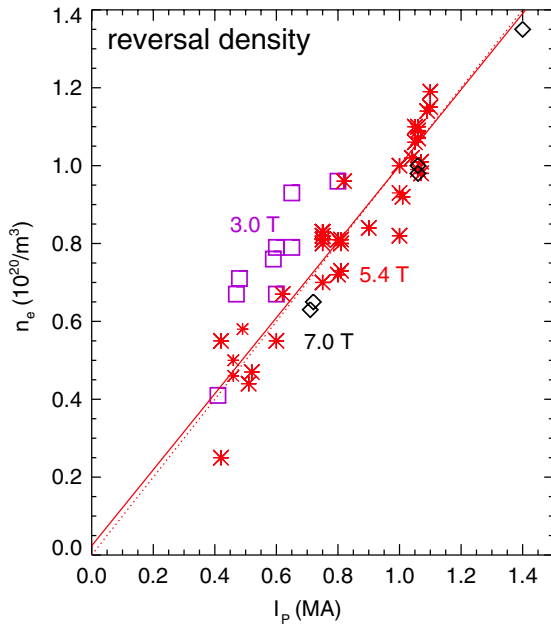
Figure 10. The density at the rotation reversal initiation time as a function of plasma current for 5.4 T (asterisks), 3.0 T (squares) and 7.0 T (diamonds) discharges. This includes LSN, USN and limited plasmas. The solid line is the best fit to the 5.4 T data, while the dotted line has a slope of unity. Smaller asterisks are from discharges with reversed current and field.

Figure 11. The density at the start of the rotation reversal as a function of $1/q$ ($1/q_{95}$ for diverted discharges) for 7.0 T (diamonds), 5.4 T (asterisks), 4.1 T (dots), 3.5 T (triangles) and 3.0 T (squares) discharges. The dotted line represents $3.5/q$, which is a good approximation to the 5.4 T points.

of LSN, USN and limited discharges; magnetic configuration does not seem to affect the reversal density. Some of the scatter is because plasmas with both upward and downward density ramps have been included, and as has been seen in figure 4, there is a hysteresis of about 10% in density. Included in the 5.4 T data set are discharges with reversed magnetic field and plasma current (shown by the smaller asterisks). These reversals occur at electron densities indistinguishable from those with normally oriented current and field. The sense of the reversals is the same, switching from the co-current direction at lower density to counter-current at higher density. Also included on the plot is the best fit line for the 5.4 T points (solid) and a nearly identical dotted line which has a slope of unity and passes through the origin. A similar trend is apparent for 3.0 T plasmas, although there is an offset, since for the same plasma current, lower magnetic field discharges have a slightly higher reversal density. Similarly, the 7.0 T points are slightly below the 5.4 T values. This suggests that q_{95} might be a better scaling parameter. Shown in figure 11 is the density at the start of the reversal as a function of the inverse of the rotational transform q, for different toroidal magnetic fields. For diverted discharges, $1/q_{95}$ has been used, while for limited plasmas, $1/q(a)$ has been taken. There is a distinct increase of the reversal density with increasing $1/q$, although since the lower field points are slightly lower, and the higher field points are slightly higher than the 5.4 T values, it indicates that the inverse magnetic field dependence is weaker than the plasma current dependence. This point is emphasized in figure 12, a plot of the reversal density as a function of toroidal magnetic field at fixed plasma current. The best fit curve is proportional to $B^{-0.6}$, weaker than the $1/B$ dependence of $1/q$. The best fit expression for the relationship
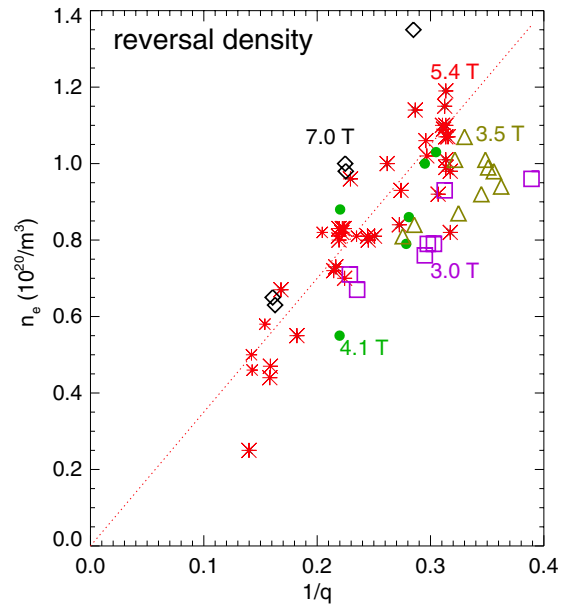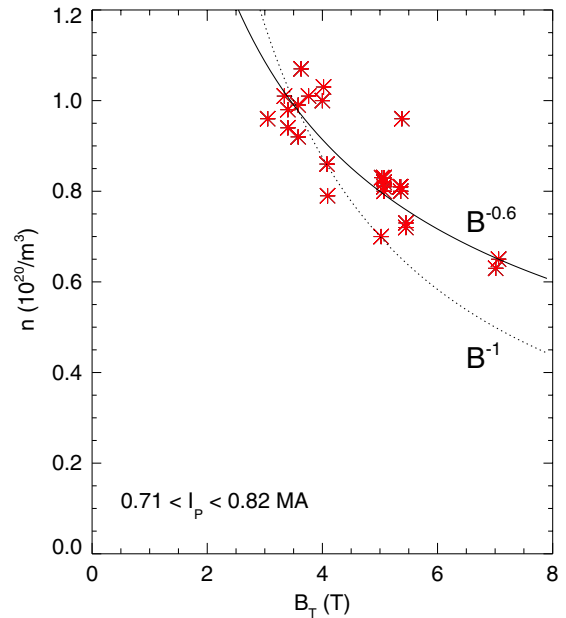

Figure 12. The reversal density as a function of magnetic field, for plasma currents between 0.71 and 0.82 MA. The solid curve is proportional to $B^{-0.6}$ and the dotted curve is proportional to $1/B$.

between the reversal density, plasma current and magnetic field can be written $n_{rev}B^{0.6}/I_p = 2.8$ with n_{rev} in 10^{20} m^{-3}, B in T and I_p in MA. A simple approximation for the 5.4 T points is $n_{rev}q_{95} = 3.5$. The magnetic field and plasma current were independently varied.

4. Rotation reversal profile evolution

In the previous section, time histories and parameter scalings of the toroidal rotation at the plasma centre were shown; in this
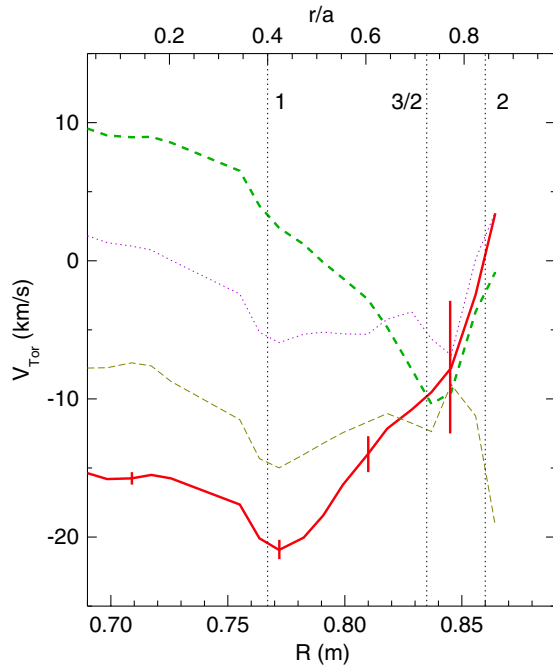
Figure 13. The toroidal rotation velocity profiles at different times for the 1.05 MA, 5.4 T ($q_{95} = 3.23$) LSN discharge shown by the dotted lines in figure 2. Dashed line, 1.10–1.28 s; dotted line, 1.32–1.34 s; dashed–dotted line, 1.36–1.38 s; solid line, 1.42–1.60 s. The vertical dotted lines indicate the locations of the $q = 1$, 3/2 and 2 surfaces. Typical statistical error bars are shown.

Figure 14. The electron temperature (top frame) and density (bottom frame) profiles from Thomson scattering before (asterisks, 1.15–1.25 s) and after (dots, 1.45–1.55 s) the rotation reversal for the discharge of figure 13.

section the evolution of the entire rotation velocity profile during reversals will be examined. Shown in figure 13 are the rotation velocity profiles at different times for the discharge shown by the dotted lines in figure 2, which underwent the reversal process between 1.3 and 1.4 s. The dashed curve represents the rotation velocity profile before (1.10–1.28 s) the reversal initiation, and is co-current in the core. The solid line indicates the velocity profile after (1.42–1.60 s) the rotation inversion and is counter-current over most of the profile. Two intermediate profiles are also shown. The reversal occurred inside of $R = 0.835$ m ($r/a \sim 0.7$), which corresponds to the location of the $q = 3/2$ surface; the profile was unchanged or anchored outside of this location. The velocity profile inside of the $q = 1$ surface was relatively flat due to sawtooth oscillations, as has been seen on TCV [11–13]. The magnetic axis for this discharge was at $R = 0.683$ m and the last closed flux surface (LCFS) was at $R = 0.894$ m. The radial electric field at $R = 0.76$ m for this plasma changed from about +5 kV m^{-1} before the reversal to around −15 kV m^{-1} afterwards. Compared with the toroidal rotation velocity profiles, there was very little change in the electron temperature and density profile shapes before and after the reversal, as shown in figure 14, a situation which has also been documented in TCV plasmas.

In order to determine if the anchoring position of the rotation velocity profile at $R = 0.835$ m in figure 13 during the core reversals is fixed at that location or is tied to the location of the $q = 3/2$ surface, discharges with different q profiles have been investigated. Shown for comparison in figure 15 are the velocity profiles at different times for the 0.8 MA, 5.4 T ($q_{95} = 4.67$) USN discharge shown by the dashed lines
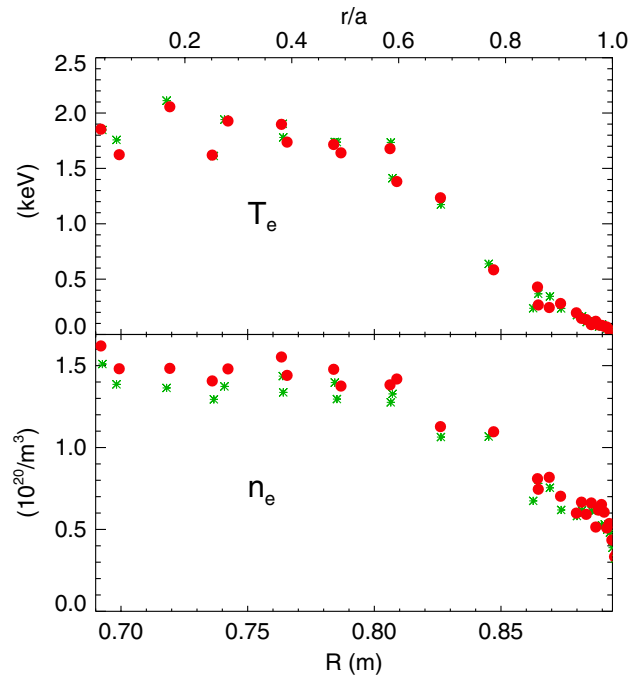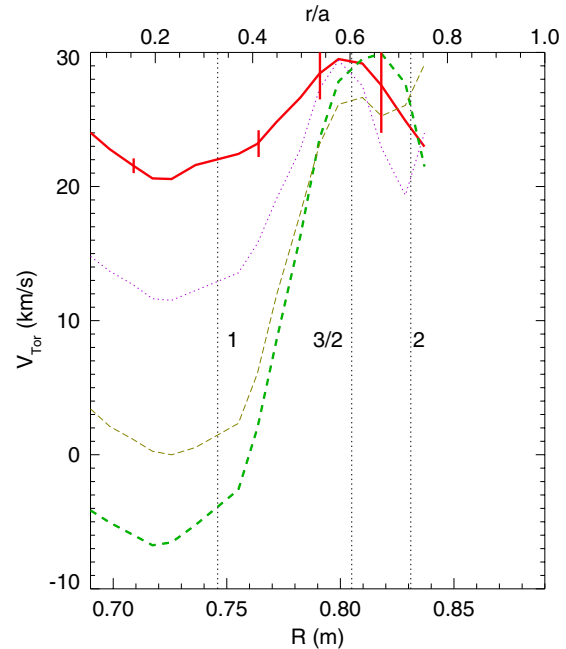

Figure 15. The rotation velocity profiles at different times for the 0.80 MA, 5.4 T ($q_{95} = 4.67$) USN discharge shown by the dashed lines in figure 8. Dashed line, 0.70–0.90 s; dotted line, 0.98–1.00 s; dashed–dotted line, 1.04–1.06 s; solid line, 1.12–1.32 s. The vertical dotted lines indicate the locations of the $q = 1$, 3/2 and 2 surfaces.

in figure 8, which underwent a rotation reversal between 0.9 and 1.1 s. The central rotation was counter-current before the reversal and switched to co-current afterwards. In this case the reversal occurred inside of $R = 0.805$ m, which for this discharge also corresponds to the location of the $q = 3/2$
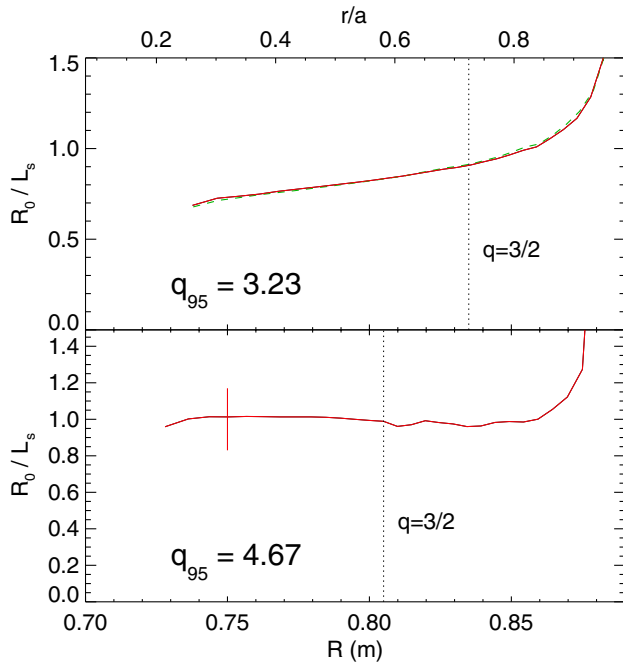
Figure 16. Inverse magnetic shear gradient scale length R/L_s profiles for the discharges of figure 13 (top, 5.4 T 1.05 MA) and figure 15 (bottom, 5.4 T 0.8 MA), before (dashed) and after (solid) the rotation reversals. The vertical dotted lines indicate the locations of the $q = 3/2$ surfaces. The vertical bar (bottom frame) gives a sense of the uncertainty in the EFIT calculations.

Figure 17. Time history comparison of four 0.64 MA limited discharges (with similar magnetic field ramps down to 3.0 T after 0.85 s) at different electron densities.

surface. These profiles were also anchored outside of $q = 3/2$ before and after the reversal, and were relatively flat at all times inside of $q = 1$. The magnetic axis was at $R = 0.676$ m and the LCFS was at $R = 0.888$ m. The question of the role of the q profile shape in the reversal process has been addressed by examining the calculated profiles from EFIT [21] reconstructions. A comparison of the inverse magnetic shear gradient scale lengths ($R_0/L_s \equiv \hat{s}/q$) for the discharges of figures 13 and 15 is shown in figure 16. The profile shapes are a little different near the $q = 3/2$ surface but the magnitudes at that location are similar, with $R/L_s \sim 1$. As seen in the top frame, there was no change in L_s before and after the rotation reversal. The largest uncertainties in the q profiles are around 10% near the mid-radius.

Information on the rotation velocity profile near the plasma edge during the reversal process is available on a very small number of discharges. In figure 17 the time histories for four 0.64 MA inner wall limited discharges are shown which all had a magnetic field ramp down to 3.0 T. The main difference between these plasmas was the electron density. The highest density discharge (dashed–dotted lines) exhibited counter-current rotation during this time interval while the lowest density plasma (dashed lines) rotated in the co-current direction. The two intermediate density discharges, shown by the solid and dotted lines, experienced rotation reversals from counter- to co-current, with the slight downward density ramps. The core rotation velocity profiles at selected times for these four discharges are shown in figure 18. The profiles before (dashed lines) and after (solid lines) the reversals are shown in the second and third frames; for the top and bottom frames, there were no inversions. Once again, the reversals occurred
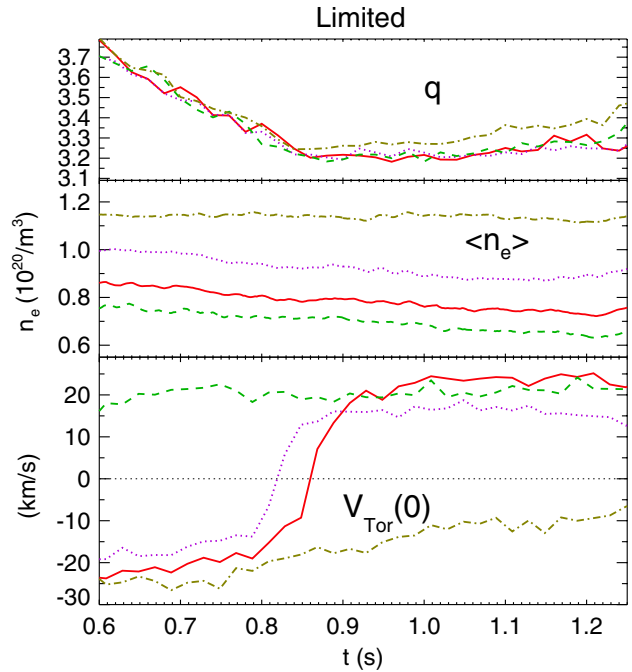
inside of the $q = 3/2$ surface and were anchored outside, and the rotation profiles were also relatively flat inside of $q = 1$. Rotation velocity profiles outside of $q = 2$ are available from the CXRS system [18] for the discharge shown by the solid lines in figure 17. Shown in figure 19 are the time histories of the toroidal rotation at four locations, $R = 0.690, 0.856, 0.867$ and 0.881 m, for the plasma shown by the solid lines in figure 17 (0.64 MA, 3.0 T limited). The solid line in figure 19 indicates the core rotation reversal, passing through zero velocity at $t = 0.86$ s. The velocity time histories near the plasma edge are shown by the symbols. The edge rotation was only available during the diagnostic neutral beam pulses, indicated in the bottom of the figure. There was a transient counter-current spike in the rotation, with a maximum at $R = 0.856$ m, as the central velocity passed through zero, but otherwise, the edge rotation was the same before and after the core reversal. There was no change at all in the velocity at $R = 0.881$ m. The edge velocity profiles for this discharge before, during and after the reversal are shown in figure 20. The edge profiles were flat immediately before (0.77 s) and after (0.93 s) the reversal, and slightly co-current; these profiles match with the core profiles in the third panel of figure 18. The maximum of the transient counter-current rotation spike was at $R = 0.86$ m, close to the $q = 2$ surface; the edge profile was anchored outside of $q = 3$. This transient occurs between the two anchor points near $q = 3/2$ and $q = 3$ for this discharge. The LCFS was at $R = 0.90$ m. It is not known if this transient rotation spike is universal. This behaviour, a pulse of momentum near the $q = 2$ surface in the direction opposite to the final core rotation direction, has been seen on at least one other discharge. Shown in figure 21 are the rotation velocity time histories at four radial locations, $R = 0.683$ m (the plasma centre), $R = 0.757$ m (near $q = 1$), $R = 0.830$ m (near $q = 3/2$) and $R = 0.849$ m
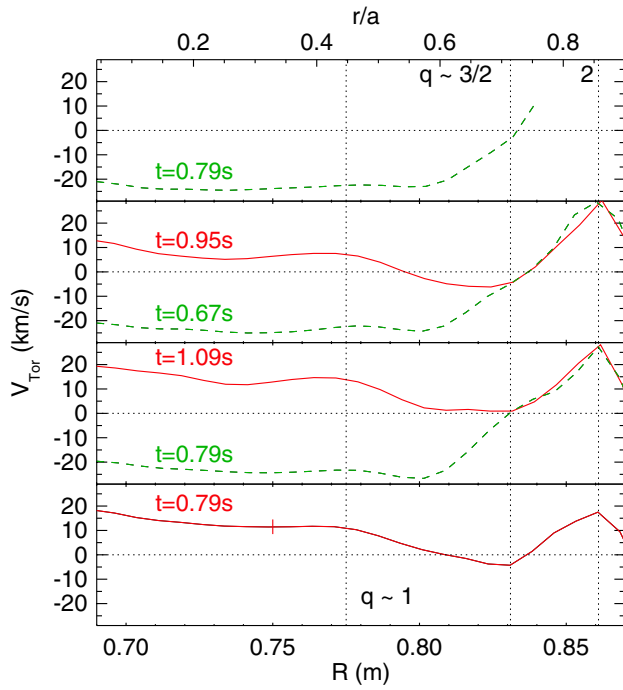
Figure 18. The rotation velocity profiles for the discharges of figure 17 (limited, 0.64 MA, 3.0 T), in order of descending density. Top frame, the dashed–dotted lines of figure 17; second frame, the dotted lines of figure 17; third frame, the solid lines of figure 17; bottom frame, the dashed lines of figure 17. The profile times are indicated. Shown by the vertical dotted lines are the locations of the $q = 1$, 3/2 and 2 surfaces. A typical error bar is shown in the bottom frame.

(near $q = 2$) for the discharge of figure 13. Inside of $q = 1$, reversal from the co- to counter-current direction is evident. Near $q = 3/2$, there was no change during the core reversal. Near the $q = 2$ surface, there was a transient spike in the direction opposite to the final core rotation direction, similar to what was seen in figure 19. It is possible that this transient rotation pulse plays a role in momentum conservation.

5. Turbulence changes during reversals

As was shown in figures 14 and 16, there was very little change in the density, temperature or q profiles (or other macroscopic parameters), while there was a drastic transformation in the toroidal velocity profiles following the rotation reversals. Significant changes in the character of density fluctuations have also been observed during rotation reversals. Shown in figure 22 are dispersion plots of density fluctuations from the PCI diagnostic [18] before and after the core reversal of the discharge shown in figures 13 and 2 (dotted lines). There are distinct lobes with $|k_R| \geqslant 2$ cm^{-1} for frequencies above 100 kHz which are apparent when the rotation was directed co-current but which disappeared after the reversal. k_R is the wave number component from the PCI view, equal to $k_\theta / \sin \zeta$, where ζ is the angle between the PCI viewing chord and the local flux surface. Shown in figure 23 is the difference between the two spectrograms of figure 22 which demonstrate the clear structure of the lobes, which are distinct with $|k_R| \geqslant 2$ cm^{-1} for frequencies above 70 kHz. The 'slope' of this feature, or apparent phase velocity, is $2\pi f/k_R \sim 3$ km s^{-1}. This structure
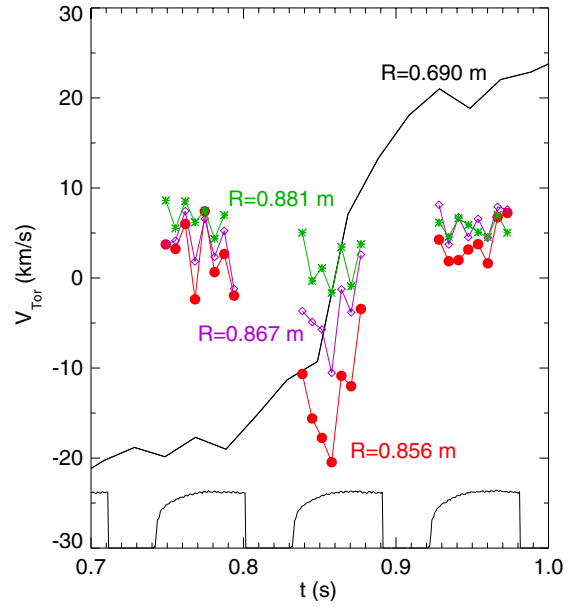

Figure 19. The toroidal rotation velocity as a function of time at $R = 0.690$ (solid line), 0.856 (dots), 0.867 (diamonds) and 0.881 (asterisks) m, for the solid line plasma of figure 17, inner wall limited at 3.0 T and 0.64 MA. At the bottom the diagnostic neutral beam pulses are shown.
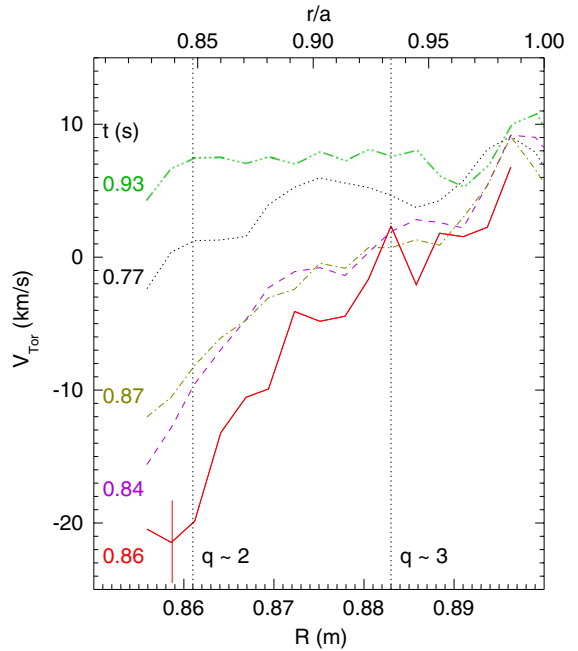

Figure 20. The edge velocity profiles at $t = 0.77$ (dotted line), 0.84 (dashed), 0.86 (solid), 0.87 (dashed–dotted) and 0.93 s (dashed–dotted–dotted–dotted line). Vertical dotted lines indicate the locations of the $q = 2$ and 3 surfaces. A typical error bar is shown.

extends up to $k_R \sim 10$ cm^{-1} and $k_R\rho_s$ is in the range from 0.15 to 0.7, typical of trapped electron modes. ρ_s is the normalized gyroradius. The feature with positive k_R has a larger intensity than that with negative k_R. The direction of propagation is unknown at this time. This feature is not visible at the plasma edge with the gas puff imaging diagnostic [18]. Since the
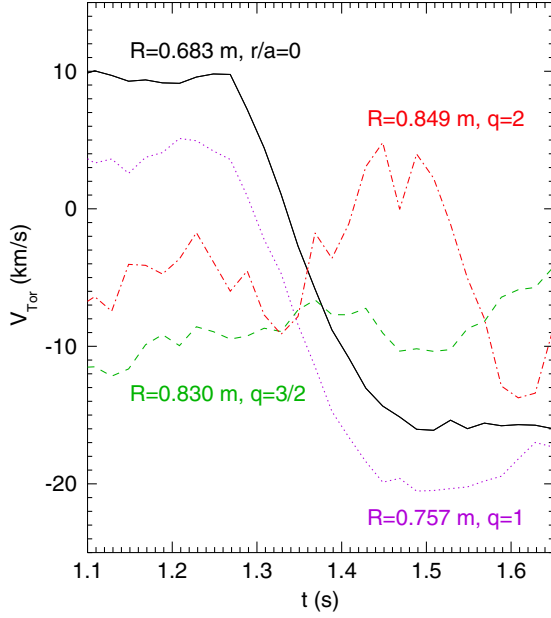
8

Figure 21. Time histories of the toroidal rotation velocity at $R = 0.683$ m (solid), $R = 0.757$ m (dotted), $R = 0.830$ m (dashed) and $R = 0.849$ m (dashed–dotted) for the discharge of figure 13.
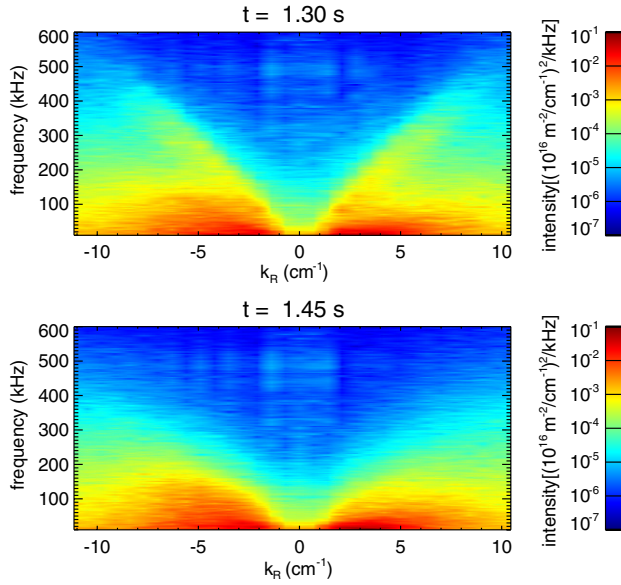

Figure 22. Dispersion plots of turbulence before (1.30 s) and after (1.45 s) the rotation reversal in the discharge shown in figure 13.

Figure 23. Difference between the two dispersion plots of figure 22, before (1.30 s) and after (1.45 s) the rotation reversal.

Figure 24. The core rotation velocity (top) and intensity of density fluctuations (bottom) above 180 kHz, sorted by k_R, as a function of time for the discharge of figures 13 and 22.

positive and negative slopes in figure 23 are the same, this also indicates that this structure exists in the plasma interior where flux surfaces are symmetric. The time evolution of these features is shown in figure 24, which depicts the intensity of fluctuations above 180 kHz as a function of time and sorted by k_R. For the fluctuations (above 180 kHz) with $k_R \sim +5$ cm^{-1}, there was an abrupt drop in intensity shortly after the core reversal begins (1.3 s). This drop is not due to a Doppler shift out of the observation range, but to a decrease in turbulence. For $k_R \sim -5$ cm^{-1} fluctuations, there was a lingering decay and a slight upshift in wavenumber magnitude. In order to highlight the correlation between the rotation reversal and
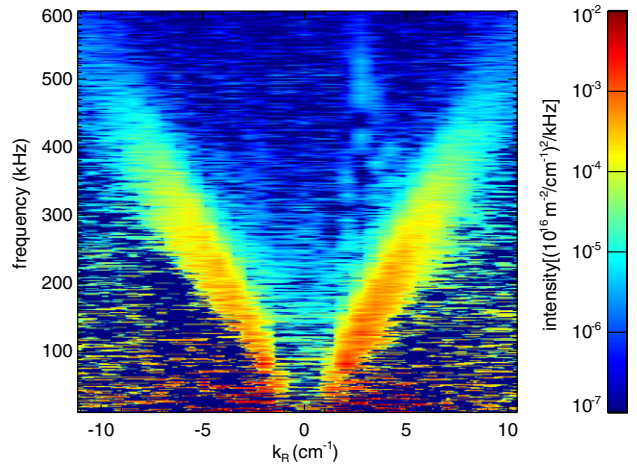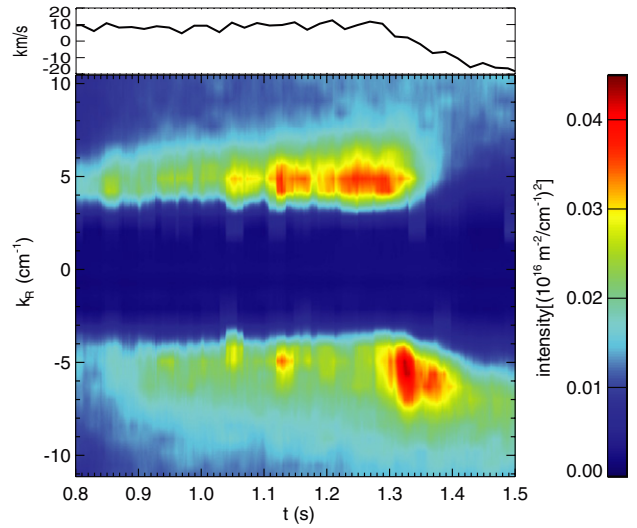
this structure in the density fluctuations, the evolution of the turbulence intensity for the three discharges of figure 2, with k_R between +4.2 and +5.6 cm^{-1} and frequency above 180 kHz, is compared with the core velocity time histories in figure 25. There was an abrupt drop in the fluctuation intensities in these features about 40 ms after the rotation reversals began.

Information on density fluctuations from reflectometry [18] is available on selected discharges. For the 88 GHz channel of this system, the cutoff density is at 0.96×10^{20} m^{-3} and for the 60 GHz channel, the cutoff is at 0.45×10^{20} m^{-3}. For a particular 5.07 T discharge with a plasma current of 0.75 MA ($q_{95} = 4.56$), the reversal density (line averaged) was 0.85×10^{20} m^{-3}. Since the density profile for this plasma was centrally peaked ($n_e(0) = 1.35 \times 10^{20}$ m^{-3}), it happens that the cutoff density for the 88 GHz channel was at $R = 0.80$ m, just inside of the $q = 3/2$ surface, while the 60 GHz channel was viewing the plasma edge. Shown in figure 26 is the complex spectrogram time evolution from the 88 GHz channel for this discharge, which underwent the rotation reversal from the co- to counter-current direction beginning at 1.11 s. There
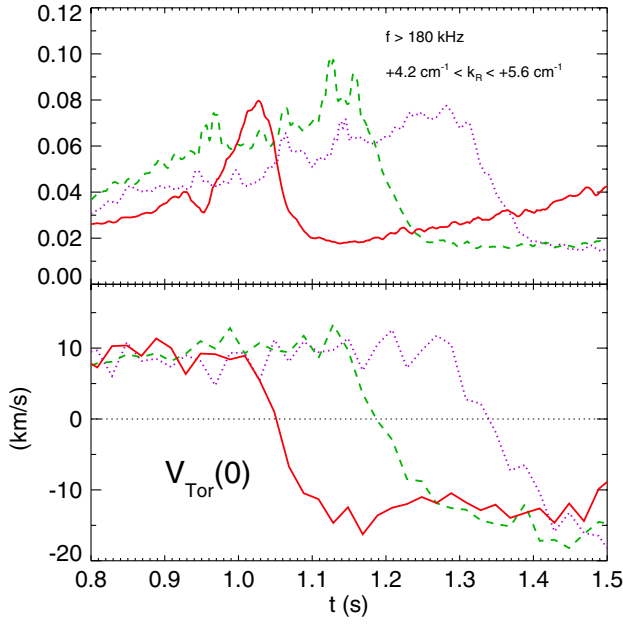
Figure 25. Density fluctuation intensities above 180 kHz and with $+4.2\,\text{cm}^{-1} \leqslant k_R \leqslant +5.6\,\text{cm}^{-1}$ (top frame) and core rotation velocities (bottom frame) as a function time for the three discharges of figure 2.
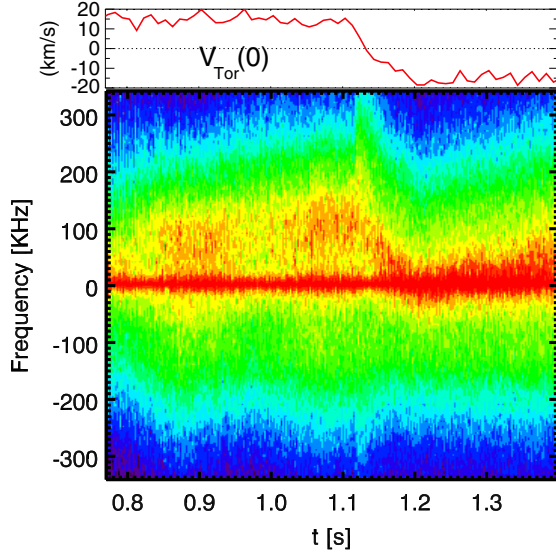

Figure 26. Core rotation velocity (top) and complex spectrogram from the 88 GHz reflectometer channel (bottom) for a $q_{95} = 4.56$ plasma which had a reversal at 1.11 s.

was a distinct drop in the 'positive' frequency fluctuations from the 88 GHz channel at this time, whereas there was no change in the signal from the outer 60 GHz channel. This supports the observation that the reversal process occurs inside of the $q = 3/2$ surface. How this manifestation of density fluctuation behaviour is related to the mode of figure 23 is unknown.

6. Discussion and conclusions

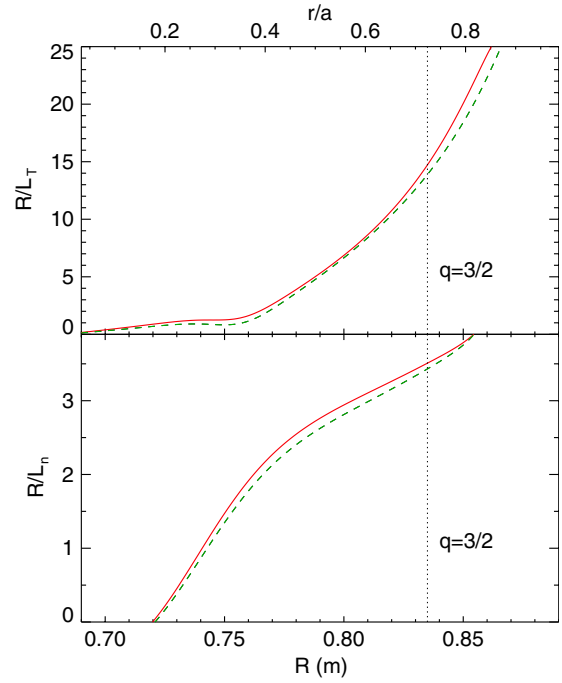In order to address the question of what can cause the toroidal rotation to switch direction while other macroscopic

Figure 27. The inverse electron temperature (top) and electron density (bottom) gradient scale lengths before (dashed) and after (solid) the rotation reversal for the discharge of figures 13 and 14. The vertical dotted line indicates the location of the $q = 3/2$ surface.

parameters remain unchanged, it is informative to examine the momentum flux. The momentum flux can be written as the sum of three terms [22],

$$- \chi_\phi \partial v_\phi / \partial r + V_\text{P} v_\phi + \Pi^{\text{res}}$$

one proportional to the momentum diffusivity χ_ϕ, the momentum pinch V_P and the residual stress Π^{res}. A change in sign of any of these could give rise to a change in direction of the toroidal rotation velocity. χ_ϕ is not likely directly involved in the reversal process because it is positive definite and cannot change sign. For both ion temperature gradient (ITG) and trapped electron mode (TEM) instabilities, the turbulent equipartition pinch [23] is directed inwards and cannot change sign unless the density gradient changes sign. Similarly, the sign of the Coriolis pinch [24] can change only if the density profile gradient changes sign. As shown in figure 14 (and in figure 27), the density gradient definitely does not change sign following the rotation reversal. For ITG turbulence, the thermoelectric pinch [23] can be either inwards or outwards, depending on the mode propagation direction and the proximity to linear marginality. However, this is only expected to play a role for large temperature gradients, such as in an H-mode pedestal, and is probably not important for core L-mode reversals. For TEM turbulence, the thermoelectric pinch can change sign for certain combinations of the values of the temperature and density gradient scale lengths [22]. However, the observed gradient scale lengths do not change before and after the reversals (see figures 14 and 27), so this is also an unlikely explanation. The temperature and density gradients used in figure 27 were taken from smooth fits to the profiles of figure 14. It can be concluded that the momentum pinch most likely does not play a role in the reversal process.
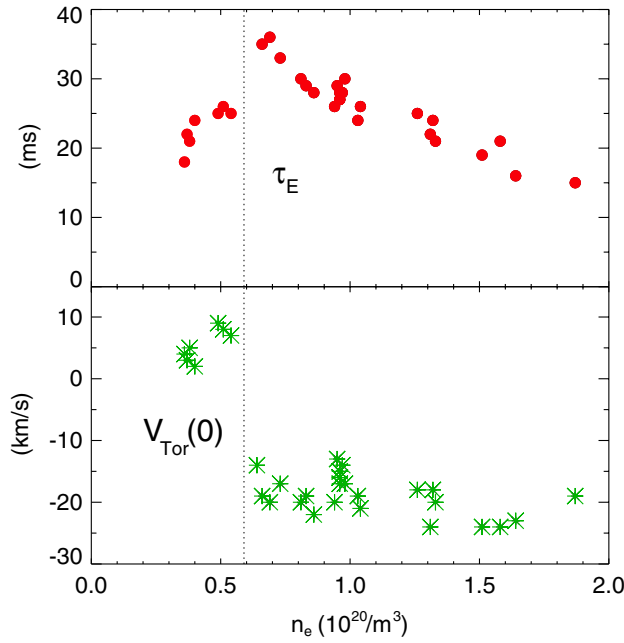
Figure 28. The global energy confinement time (top) and central toroidal rotation velocity (bottom) as a function of average electron density for a series of 0.62 MA, 5.2 T ($q_{95} = 5.0$) discharges. The vertical dotted line indicates the density which separates co- and counter-current rotation.

The residual stress can change sign depending on the nature of the underlying turbulence, such as by a change in the mode propagation direction. One example would be a change of wave propagation from the electron diamagnetic drift direction (electron drift waves) to the ion direction (ion drift waves or ITG modes) as the density exceeds a critical threshold [25]. Such a change from TEM (or ETG) to ITG turbulence domination has been invoked to explain the transition in global energy confinement from the linear (neo-Alcator) to saturated ohmic confinement regimes [26]. In fact, the reversal density of $\sim 0.8 \times 10^{20}$ m^{-3} for 5.4 T, 0.8 MA discharges (figure 10) is in the range of the density separating the linear energy confinement regime from the saturated confinement regime for ohmic discharges (figure 1 of [26]). This connection is emphasized in figure 28 which shows the global energy confinement time (from magnetics) and the core toroidal rotation velocity as a function of electron density for the series of 0.62 MA, 5.2 T discharges shown in figure 1. The density of the rotation reversal is very close to the density which separates the linear increase in global energy confinement from the saturated confinement regime, around 0.6×10^{20} m^{-3} for these conditions. This relationship holds for discharges at different plasma currents as well. A comparison of the rotation reversal density and the transition density from the linear to saturated ohmic confinement regime, for several different plasma conditions, is shown in figure 29. There is a very good correlation between these two over a factor of two in density, suggesting a common underlying mechanism. Unfortunately the propagation direction of the feature which is present during the co-current rotation (figure 23) has not yet been determined. If this propagates in the electron diamagnetic drift direction, then the co-current plasma rotation and linear energy confinement would be consistent with CTEM domination of the turbulence at low density.
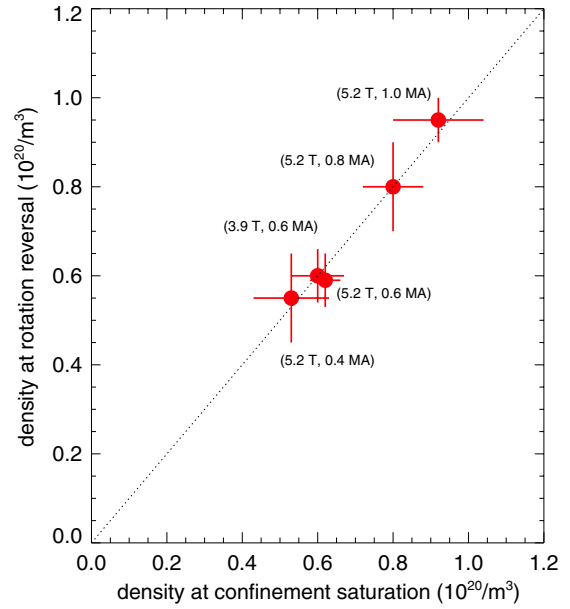

Figure 29. The rotation reversal density as a function of the transition density between linear and saturated energy confinement. Magnetic fields and plasma currents for each point are listed. The dotted line has a slope of unity.
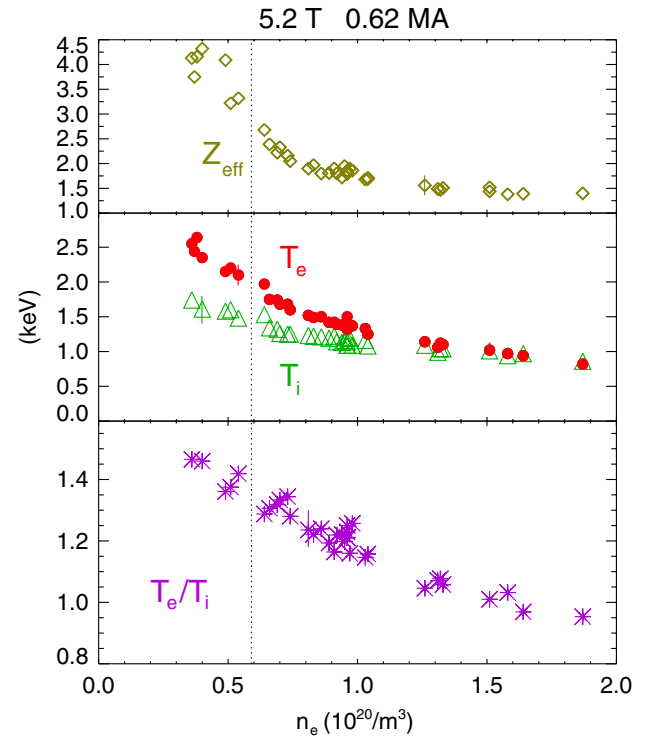

Figure 30. Z_{eff} (top), the electron (dots) and ion (triangles) temperatures (middle) and T_e/T_i ratio (bottom) as a function of average electron density for the series of 0.62 MA, 5.2 T discharges shown in figure 28. The vertical dotted line indicates the density which separates co- and counter-current rotation. Typical error bars are shown.

Other parameters which are known to have an effect on the underlying turbulence, and might be involved in the confinement regime change and rotation reversal process have been considered. For the discharges of figure 28, there was
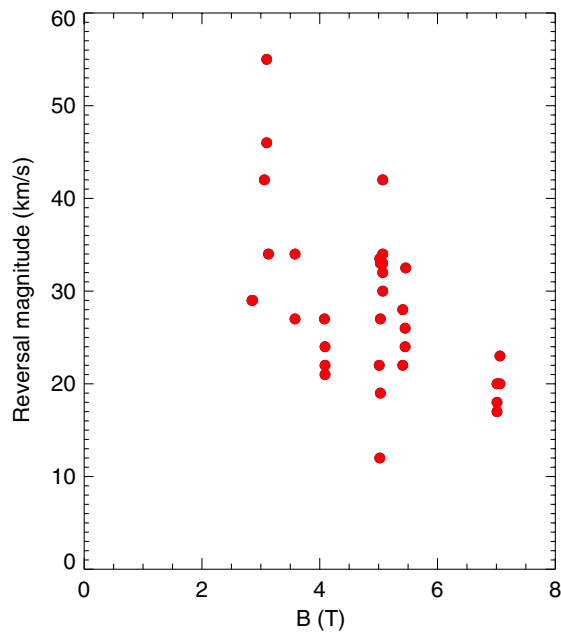
Figure 31. The magnitude of the rotation reversal velocity change as a function of the toroidal magnetic field.

a monotonic drop in $Z_{\rm eff}$, the electron and ion temperatures, and the temperature ratio with increasing density, as can be seen in figure 30. The values of $Z_{\rm eff}$ and the ratio of $T_{\rm e}/T_{\rm i}$ were 2.8 and 1.35, respectively, when the rotation switched from co- to counter-current and the global energy confinement made the transition from the linear to saturated regime. This continuous behaviour through the 'transition' density is in contrast to the abrupt changes which occur with the rotation and energy confinement. For 1.0 MA discharges, with a higher reversal density, the values for $T_{\rm e}/T_{\rm i}$ and $Z_{\rm eff}$ at the reversal and confinement change were somewhat lower, 1.26 and 2.1, respectively.

The strong correlation between rotation reversals, confinement regime change and turbulence behaviour suggests that all three are intimately related. The feature of figure 23 is only apparent when the rotation is in the co-current direction and the energy confinement is in the linear regime, and then disappears when the rotation switches to the counter-current direction and the energy confinement saturates. The rotation reversal is most likely associated with a change in sign of the residual stress when this structure disappears.

Open questions which need to be addressed include: how is momentum conserved during the reversal process? What is the role of the $q = 3/2$ surface? Why does the reversal density scale linearly with plasma current, and as $B^{-0.6}$? Is there a connection between the reversal density, the density of confinement saturation and the minimum density in the L–H power threshold? What determines the magnitude of the hysteresis in density? What determines the magnitude of the reversal velocity? Regarding the last question, there is

some evidence that the magnitude of the reversal is larger for lower toroidal magnetic field plasmas. Shown in figure 31 is the magnitude of the reversal velocity change as a function of toroidal magnetic field.

In summary, direction reversals of intrinsic toroidal rotation have been observed in Alcator C-Mod ohmic L-mode plasmas following modest electron density or toroidal magnetic field ramps. The reversal process occurs in the plasma interior, inside of the $q = 3/2$ surface. For low density plasmas, the rotation is in the co-current direction, and can reverse to the counter-current direction following an increase in the electron density above a certain threshold. Reversals from the co- to counter-current direction are correlated with a sharp decrease in density fluctuations with $k_R \geqslant 2\,{\rm cm}^{-1}$ and frequencies above 70 kHz. The density at which the rotation reverses increases linearly with plasma current, and decreases with increasing magnetic field. There is a strong correlation between the reversal density and the density at which the global ohmic L-mode energy confinement changes from the linear to the saturated regime.

Acknowledgments

References

[1] Terry P.W. 2000 *Rev. Mod. Phys.* **72** 109
[2] Hahm T.S. 1994 *Phys. Plasmas* **1** 2940
[3] Burrell K. 1997 *Phys. Plasmas* **4** 1499
[4] Strait E.J. *et al* 1994 *Phys. Rev. Lett.* **74** 2483
[5] Rice J.E. *et al* 2007 *Nucl. Fusion* **47** 1618
[6] Nave M.F.F. *et al* 2010 *Phys. Rev. Lett.* **105** 105005
[7] Romannikov A. *et al* 2000 *Nucl. Fusion* **40** 319
[8] Rice J.E. *et al* 2005 *Nucl. Fusion* **45** 251
[9] Rice J.E. *et al* 2008 *Plasma Phys. Control. Fusion* **50** 124042
[10] Eriksson L.-G. *et al* 2009 *Plasma Phys. Control. Fusion* **51** 044008
[11] Bortolon A. *et al* 2006 *Phys. Rev. Lett.* **97** 235003
[12] Duval B.P. *et al* 2007 *Plasma Phys. Control. Fusion* **49** B195
[13] Duval B.P. *et al* 2008 *Phys. Plasmas* **15** 056113
[14] Marmar E.S. *et al* 2007 *Fusion Sci. Technol.* **51** 261
[15] Rice J.E. *et al* 1997 *Nucl. Fusion* **37** 421
[16] Ince-Cushman A. *et al* 2008 *Rev. Sci. Instrum.* **79** 10E302
[17] Rice J.E. *et al* 2004 *Nucl. Fusion* **44** 379
[18] Basse N.P. *et al* 2007 *Fusion Sci. Technol.* **51** 476
[19] McDermott R.M. *et al* 2009 *Phys. Plasmas* **16** 056103
[20] Lee W.D. *et al* 2003 *Phys. Rev. Lett.* **91** 205003
[21] Lao L.L. *et al* 1985 *Nucl. Fusion* **25** 1611
[22] Diamond P.H. *et al* 2009 *Nucl. Fusion* **49** 045002
[23] Hahm T.S. *et al* 2007 *Phys. Plasmas* **14** 072302
[24] Peeters A. *et al* 2007 *Phys. Rev. Lett.* **98** 265003
[25] Diamond P.H. *et al* 2008 *Phys. Plasmas* **15** 012303
[26] Lin L. *et al* 2009 *Plasma Phys. Control. Fusion* **51** 065006